

Airy distribution: Experiment, large deviations, and additional statistics

Tal Agranov^{1,*}, Pini Zilber,¹ Naftali R. Smith,¹ Tamir Admon,² Yael Roichman^{2,3,†} and Baruch Meerson^{1,‡}¹*Racah Institute of Physics, Hebrew University of Jerusalem, Jerusalem 91904, Israel*²*Raymond and Beverly Sackler School of Chemistry, Tel Aviv University, Tel Aviv 6997801, Israel*³*Raymond and Beverly Sackler School of Physics and Astronomy, Tel Aviv University, Tel Aviv 6997801, Israel*

(Received 22 August 2019; revised manuscript received 6 November 2019; accepted 13 January 2020; published 19 February 2020)

The Airy distribution (AD) describes the probability distribution of the area under a Brownian excursion. The AD is prominent in several areas of physics, mathematics, and computer science. Here we use a dilute colloidal system to directly measure the AD in experiment. We also show how two different techniques of theory of large deviations, the Donsker-Varadhan formalism and the optimal fluctuation method, manifest themselves in the AD. We advance the theory of the AD by calculating, at large and small areas, the position distribution of a Brownian excursion conditioned on a given area and measure its mean in the experiment. For large areas, we uncover two singularities in the large-deviation function, which can be interpreted as dynamical phase transitions of third order. For small areas the position distribution coincides with the Ferrari-Spohn distribution, and we identify the reason for this coincidence.

DOI: [10.1103/PhysRevResearch.2.013174](https://doi.org/10.1103/PhysRevResearch.2.013174)

Brownian motion came to prominence in physics and other sciences with the theoretical works of Einstein [1], von Smoluchowski [2], and Langevin [3] and the experimental work of Perrin [4]. Today, more than 100 years since those remarkable discoveries, Brownian motion is a central paradigm in a multitude of fields [5,6]. Here we focus on some interesting properties of conditioned Brownian motions as described by the Airy distribution and by its extensions that we will introduce.

Since its discovery nearly four decades ago [7,8], the Airy distribution (AD) keeps reappearing in seemingly unrelated problems in different fields of science. One of its first applications was to inventory problems where the AD describes, for example, the distribution of the time spent by locomotives in a railway depot [9,10]. The AD appears in the description of the computational cost of data storage algorithms [11]. In graph theory the AD is the distribution of the internal length of a rooted planar tree [10]. More recently, the AD appeared in physics: as the distribution of the maximal height of fluctuating interfaces [12–14], the avalanche size distribution in sandpile models [15], the size fluctuations of ring polymers [16], and the position distribution of laser cooled atoms [17]. See Ref. [5] for a review of some of these examples.

Despite its importance, the measurement of the AD in an experiment is lacking. Here we report such measurements in the simplest setting where the AD was originally discovered [7,8]: the area under a Brownian excursion $x(t)$ in one dimension. We also advance the theory of, and experiments on, the AD by focusing on its large-deviation properties. We show how two different large-deviation formalisms manifest themselves in the AD. This allows us to probe an important quantity: the position distribution of a Brownian excursion conditioned on a specified area.

Consider a Brownian excursion: a Brownian motion $x(t)$, conditioned to start and end at the origin $x(t=0) = x(t=T) = 0$ and to stay positive $x(t) > 0$ for $0 < t < T$. The area under the Brownian excursion

$$A = \int_0^T x(t) dt \quad (1)$$

is a random variable characterized by the probability distribution $P(A, T)$: the AD. The only dimensional parameters entering the problem are A , T , and the particle diffusivity D_0 ,¹ and dimensional analysis yields

$$P(A, T) = \frac{1}{\sqrt{D_0 T^3}} f\left(\frac{A}{\sqrt{D_0 T^3}}\right). \quad (2)$$

The Laplace transform of the scaling function f , found by probabilistic methods [7,8], was formally inverted to give the

*tal.agranov@mail.huji.ac.il

†roichman@tauex.tau.ac.il

‡meerson@mail.huji.ac.il

Published by the American Physical Society under the terms of the [Creative Commons Attribution 4.0 International](https://creativecommons.org/licenses/by/4.0/) license. Further distribution of this work must maintain attribution to the author(s) and the published article's title, journal citation, and DOI.

¹The Brownian motion can be formally defined by the equation $\dot{x} = \sqrt{D_0} \xi(t)$, where $\xi(t)$ is a δ -correlated zero-mean Gaussian noise ($\langle \xi(t) \xi(t') \rangle = \delta(t - t')$).

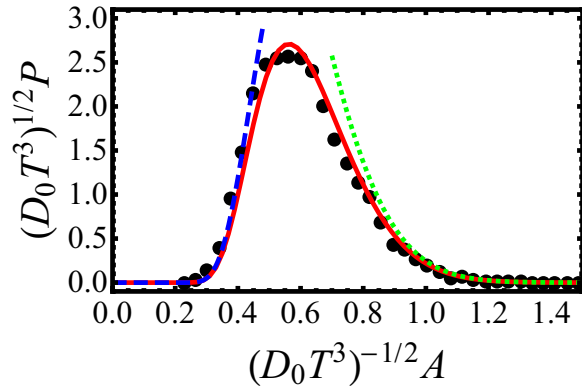


FIG. 1. The solid line shows $f(\xi)$ from Eq. (3). The symbols represent the experimentally measured histogram of the area under 12 240 excursions of duration $T \simeq 33.3$ s. The dashed and dotted lines show the small- and large-area tails (4) and (5), respectively, but with account of preexponential corrections, calculated in Ref. [20].

closed analytic form [10]

$$f(\xi) = \frac{2\sqrt{6}}{\xi^{10/3}} \sum_{k=1}^{\infty} e^{-\beta_k/\xi^2} \beta_k^{2/3} U(-5/6, 4/3, \beta_k/\xi^2), \quad (3)$$

where $U(\dots)$ is the confluent hypergeometric function [18], $\beta_k = 2\alpha_k^3/27$, and α_k are the ordered absolute values of the zeros of the Airy function $\text{Ai}(\xi)$ [19]. The Laplace transform of f was also obtained by using path-integral techniques [13]. The function $f(\xi)$ is shown in Fig. 1.

The expression (3) is quite complicated. As a result, calculating the moments of the AD is already challenging [21]. Here we will focus on the AD's tails [22,23]

$$-\ln P(A, T) \simeq \begin{cases} \frac{2\alpha_1^3}{27} \frac{D_0 T^3}{A^2}, & A \ll \sqrt{D_0 T^3} \\ \frac{6A^2}{D_0 T^3}, & A \gg \sqrt{D_0 T^3}, \end{cases} \quad (4)$$

which are depicted, with account of preexponential factors, calculated in Ref. [20], in Fig. 1. They correspond to very small or very large values of the dimensionless parameter $\tilde{A} \equiv AD_0^{-1/2}T^{-3/2}$, which plays a key role in this paper. As we show here, these tails are intimately connected with two different large-deviation formalisms of statistical mechanics. These formalisms provide a physical picture behind these tails by characterizing the most relevant particle trajectories, which we were also able to measure in the experiment.

Our experimental setup is made of colloidal suspensions of silica spheres in water ($1.50 \pm 0.08 \mu\text{m}$ in diameter, mass density of 2.0 g/cm^3 , Polysciences lot No. A762412), which are loaded into a sample cell of dimensions $22 \times 22 \times 0.04 \text{ mm}^3$ constructed from a microscope slide and a coverslip. The particles are then allowed to sediment and equilibrate and diffuse close to the bottom slide for 30 min at room temperature before measurements start. Quasi-2D monolayers of area fractions $\phi = 0.069 \pm 0.005$ and $\phi = 0.062 \pm 0.005$ are prepared by diluting the original suspension with double-distilled water (18 M Ω). Sample walls are coated with bovine serum albumin to avoid particle attachment to the bottom wall of the cell. Particle position and motion in the plane perpendicular to the optical axis are observed using bright field

microscopy (Olympus IX71). Images are captured by a complementary metal-oxide semiconductor camera (Grasshopper 3, Point Grey Research) at a rate of 30 frames/sec to allow for easy particle tracking. Conventional single-particle-tracking techniques were used to extract particle location with an accuracy of 6 nm [24]. The particle diffusivity was evaluated from the particle's mean-square displacement $D_0 = \langle \Delta x^2(t) \rangle / 2t$ averaged over all particles in the ensemble. Excursions are constructed from the trajectories using the Vervaat transform (see Appendix A for details).

Figure 1 presents the measured histogram of the area under excursions of the colloidal particles. It shows good agreement with Eqs. (2) and (3). The histogram is a bit broader than the theoretical distribution in the region of the maximum. This effect is explained by the small but finite polydispersity of the particle diameters, leading to small variations of their diffusivity.

To start our large-deviation analysis, let us define the rescaled area $a = A/T$, which is the time-averaged position of the Brownian excursion. At fixed a , the small- A limit (4) corresponds to very long times $T \gg a^2/D_0$, whereas the large- A limit (5) corresponds to very short times $T \ll a^2/D_0$.

Let us start with the small- A (or long-time) limit. We argue that the distribution of a obeys a large-deviation principle due to Donsker and Varadhan [25–28], where the long-time probability of observing any finite a decays exponentially with time:

$$-\ln P(a \ll \sqrt{D_0 T}) \simeq TI(a). \quad (6)$$

From dimensional analysis, the rate function $I(a)$ scales as D_0/a^2 , already reproducing the correct scaling behavior (4) of the small- A tail. Reproducing the numerical factor $2\alpha_1^3/27$ takes slightly more effort. It requires determining the ground state energy of a Schrödinger-type tilted operator, obtained from the generator of the constrained Brownian excursion [25,26]. We present this calculation in detail in Appendix B. The trajectories $x(t)$, which mostly contribute to the small- A tail (4), stay close to the origin, without ever crossing it, for a long time. As we show below, the position distribution, characterizing these trajectories, is stationary for most of the time, which explains the exponential decay of P with time [see Eq. (6)]. Figure 2(a) presents the experimentally measured average position of trajectories with small A , which is almost constant in time, as expected.

The large- A tail (5) is markedly different. It is dominated by a single most probable excursion which realizes the prescribed large A by straying far away from the origin during a very short time. Other trajectories with the same A have exponentially smaller probabilities. This optimal trajectory $x_A^*(t)$ can be found by the optimal fluctuation method (OFM). For the Brownian motion, the OFM becomes geometrical optics [30–36]. The starting point of the OFM is the path probability measure of a Brownian trajectory $x(t)$. It is given, up to preexponential factors, by the Wiener action $\mathcal{P}[x(t)] \propto \exp(-s/D_0)$, where

$$s[x(t)] = \frac{1}{2} \int_0^T dt \dot{x}^2(t). \quad (7)$$

The optimal trajectory can be found by minimizing the action (7) along excursions $x(t)$ subject to the constraint (1).

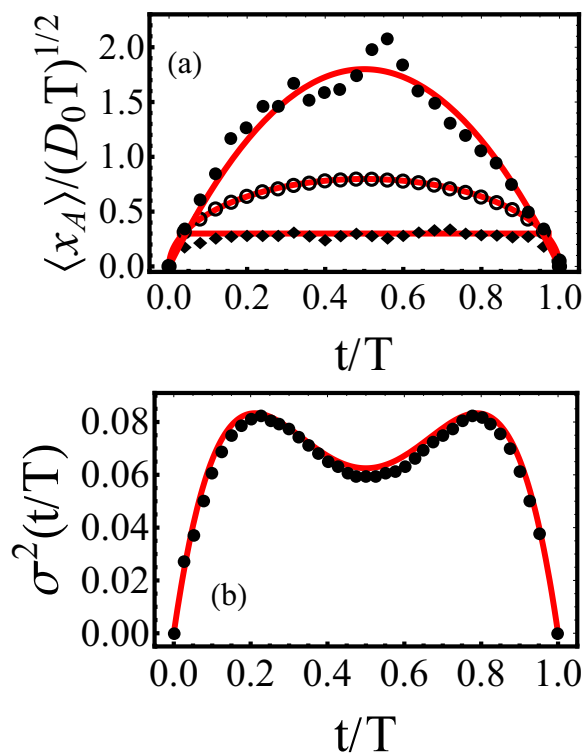


FIG. 2. (a) Rescaled position averages of the experimentally measured excursions, conditioned on a moderately large area $\tilde{A} = 1.2 \pm 0.05$ (closed circles) and small area $\tilde{A} = 0.3 \pm 0.05$ (closed diamonds). The top and bottom lines are theoretical predictions: Eq. (8) with $\tilde{A} = 1.2$ for the large area and the constant $\langle x_A \rangle / (D_0 T)^{1/2} \simeq \tilde{A} = 0.3$ for the small area. Also shown is the rescaled average position of all (that is, unconstrained) excursions (open circles) and the theoretical prediction [29] $\langle x(t) \rangle / (D_0 T)^{1/2} = \sqrt{8/\pi} [(t/T)(1 - t/T)]^{1/2}$ (middle line). Out of a total of 12 240 unconditioned excursions, there were 22 excursions within the large-area window and 200 within the small-area window. (b) Rescaled variance of simulated excursions, conditioned on a moderately large area $\tilde{A} = 1.2 \pm 0.0075$ (closed circles). The line is the theoretical prediction (18). An accurate estimation of the variance requires a very large number of trajectories. These were easier to generate in simulations than in experiment.

The latter can be accommodated via a Lagrange multiplier λ , leading to an effective Lagrangian $L(x, \dot{x}) = \dot{x}^2/2 - \lambda x$. The optimal trajectory is a parabola,

$$x_A^*(t) = (6At/T^2)(1 - t/T), \quad (8)$$

where we have imposed $x(0) = x(T) = 0$ and set $\lambda = 12A/T^3$ to obey Eq. (1). Further, $x_A^*(t)$ is also the average position over all trajectories with the large prescribed A . Figure 2(a) compares Eq. (8) with the experimentally measured average position of excursions with large A . Although the OFM becomes asymptotically exact only in the limit of $\tilde{A} \gg 1$, good agreement is observed already for $\tilde{A} \gtrsim 1$.

Plugging Eq. (8) into the action (7), we exactly reproduce Eq. (5) (see also Refs. [36,37]). The large- A tail (5) is shared by other Brownian motions (such as the Brownian bridge and its absolute value [38]) which start at $x = 0$ at $t = 0$ and return to $x = 0$ at $t = T$, but are allowed to reach or even cross $x = 0$

at $0 < t < T$. The large- A tails coincide because the optimal trajectory (8) is unaffected by the noncrossing constraint.

A more detailed characterization of the trajectories with specified area is given by the position distribution of the excursion $p[x_A(t) = X|A, T] \equiv p_A(X, t)$ conditioned on a given area $\int_0^T x_A(t) dt = A$. This important distribution has been previously inaccessible.² As we show now, the two large-deviation techniques that describe the two tails of $f(\xi)$ allow one to evaluate p_A at small and large A . From dimensional analysis, the distribution must have the scaling form

$$p_A(X, t) = \frac{T}{A} \tilde{p}_{\tilde{A}}\left(\frac{XT}{A}, \frac{t}{T}\right). \quad (9)$$

At $\tilde{A} \ll 1$, the conditional distribution can be found with the Donsker-Varadhan (DV) formalism [45] (see Appendix B). Apart from narrow temporal boundary layers at $t = 0$ and $t = T$, this formalism predicts the stationary position distribution

$$\tilde{p}_{\tilde{A}}\left(z, \frac{t}{T}\right) \simeq \frac{2\alpha_1}{3} \frac{\text{Ai}^2\left(\frac{2\alpha_1}{3}z - \alpha_1\right)}{[\text{Ai}'(-\alpha_1)]^2}, \quad \tilde{A} \ll 1, \quad (10)$$

where $\text{Ai}'(z) \equiv (d/dz)\text{Ai}(z)$. The first moment of the distribution (10) is equal to unity, which gives $\langle x_A(t) \rangle \simeq A/T$ in the dimensional variables. Figure 3(a) shows good agreement between the distribution of simulated excursions, conditioned by the small area, and Eq. (10). Simulation details are described in Appendix A. See also Fig. 2(a) for a comparison of the mean which we measured in the experiment.

The distribution (10) is known as the Ferrari-Spohn (FS) distribution. It first appeared in the studies of position fluctuations of a Brownian excursion, conditioned to stay away from a wall $x_w(t)$ which moves, sufficiently fast, back and forth so that $x_w(0) = x_w(T) = 0$ and $x_w(0 < t < T) > 0$ [46–48]. For a parabolic $x_w(t)$,

$$x_w(t) = Ct(1 - t/T), \quad (11)$$

the small- A distribution (10) and the FS distribution [48] coincide. This unexpected coincidence can be explained by an exact mapping that we found between the two systems. The details of calculation are presented in Appendix C. The mapping involves a biased ensemble [49]: an ensemble of excursions, where the probability of each excursion is reweighted by the exponential factor $e^{-\mu A[x(t)]}$, where $A[x(t)]$ is the area of the excursion. This ensemble and the ensemble of excursions conditioned on A are equivalent and they obey the same relation as the one between the canonical and microcanonical ensembles, respectively, in equilibrium statistical mechanics [49]. If we denote by $p(X, t; \mu)$ the position distribution in the biased ensemble and by $p_C(X, t)$ the position distribution of the particle relative to the parabolic wall (11) in the FS problem, the mapping reads $p(X, t; \mu = 2C/D_0T) = p_C(X, t)$ (see Appendix C). The FS distribution has also appeared in other systems [35,50–53], which is indicative of a universality class.

²Methods like Doob's h -transform [39] are hard to use due to the conditioning on both X and A [40,41]. An alternative method, proposed for a generalized Brownian bridge [42–44], could not be extended to excursions, as it is restricted to Gaussian processes.

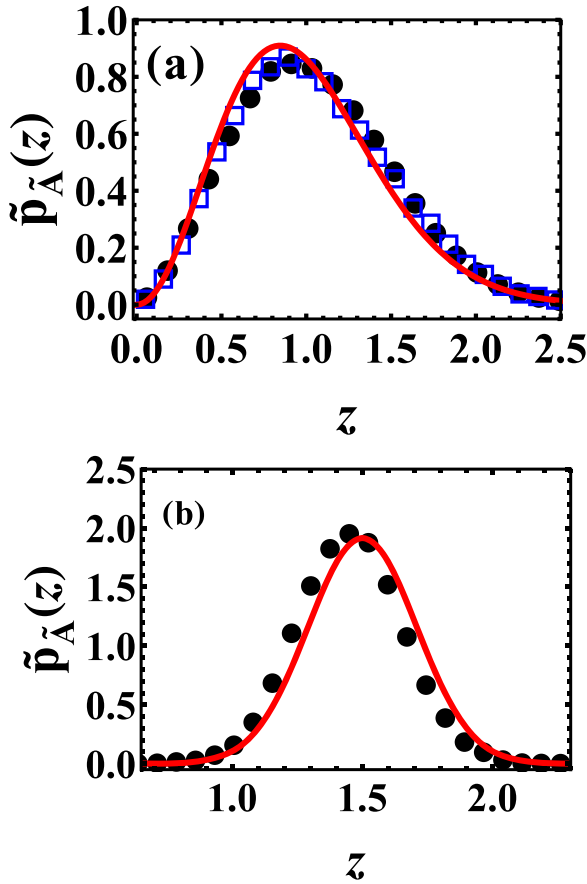


FIG. 3. Closed circles represent the position histograms $\tilde{p}_{\tilde{A}}(z, 1/2)$ of simulated excursions conditioned on A for (a) small area $\tilde{A} = 0.3 \pm 0.0075$ and (b) large area $\tilde{A} = 1.2 \pm 0.0075$. Lines are the theoretical predictions from (a) (10) and (b) (14) and (15). In the latter prediction the normalization factor was accounted for. Panel (a) also shows the histogram at $t/T = 3/4$ (open squares), confirming the time independence of the position distribution at small areas.

At $\tilde{A} \gg 1$ the conditional distribution $\tilde{p}_{\tilde{A}}(z, t/T)$ is time dependent and it can be found with the OFM (see Appendix D). The probability of an excursion to reach a specified position $x(t) = X$ and to have a given large area A comes from the optimal trajectory which minimizes the action (7) under the two constraints. The optimal trajectory consists of two parabolic segments, joined at time t with a corner singularity there, which originates from conditioning on the specified position at time t (see Appendix D). For the particular case of conditioning on the position $x = X$ at $t = T/2$, the optimal trajectory is

$$x(t') = X + (6a - 4X) \left| 1 - \frac{2t'}{T} \right| - (6a - 3X) \left(1 - \frac{2t'}{T} \right)^2 \quad (12)$$

(recall that $a = A/T$). This trajectory is shown, for several values of X , in Fig. 4(a).

However, the solution (12) is a legitimate Brownian excursion only when X is smaller than a critical value $X_{c1} = 3a$. For $X > 3a$, $x(t')$ from Eq. (12) would cross the origin, which

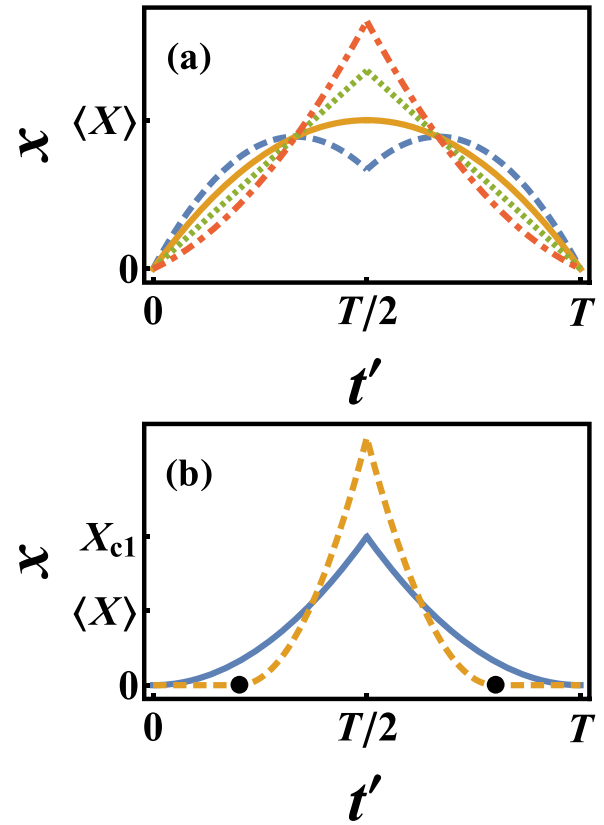


FIG. 4. Optimal paths conditioned on $x(t = T/2) = X$ and the area A , in the (a) subcritical and (b) supercritical regimes [see Eqs. (12) and (13)]. The parameters are (a) $XT/A = 1, 3/2, 2,$ and $5/2$ (dashed, solid, dotted, and dot-dashed lines, respectively) and (b) $XT/A = 3$ and 5 (solid and dashed lines, respectively). Circles show the points $|T/2 - t'| = 3A/2X$.

is forbidden. The correct solution for $X > 3a$ is provided by the tangent construction of the calculus of one-sided variations [54] and we obtain

$$x(t') = \begin{cases} \frac{4X^3}{9A^2} \left(\frac{3A}{2X} - \left| \frac{T}{2} - t' \right| \right)^2, & \left| \frac{T}{2} - t' \right| \leq \frac{3A}{2X} \\ 0, & \left| \frac{T}{2} - t' \right| \geq \frac{3A}{2X} \end{cases} \quad (13)$$

[see Fig. 4(b)]. The conditional distribution is given by Δs : the difference between the action (7) along the additionally constrained trajectory (12) or (13) and the action along the optimal trajectory (8) constrained by the area alone. As a result,

$$-\ln \tilde{p}_{\tilde{A}} \left(z, \frac{1}{2} \right) \simeq \frac{\Delta s}{D_0} = \frac{A^2}{D_0 T^3} g(z), \quad \tilde{A} \gg 1. \quad (14)$$

The large-deviation function

$$g(z) = \begin{cases} 8(z - 3/2)^2, & 0 < z \leq 3 \\ (8/9)z^3 - 6, & z \geq 3 \end{cases} \quad (15)$$

has a singularity: Its third derivative is discontinuous at $z = 3$. This singularity can be interpreted as a dynamical phase transition of the third order. Similar singularities have been recently found in other Brownian motions pushed into large-deviation regimes by constraints [33–36]. A sharp transition,

however, appears only in the limit of $\tilde{A} \rightarrow \infty$ and is smoothed out at finite \tilde{A} .

The subcritical result (15) describes Gaussian fluctuations around the mean value $\bar{z} = 3/2$ which corresponds to an excursion conditioned on A but not on X . This result is in good agreement with simulations [see Fig. 3(b)]. In the supercritical regime (16), the support of the optimal trajectory is shorter than T [see Fig. 4(b)]. As a result, the time T cannot enter the final result. This and the scaling relation (14) explain the fact that the first term in Eq. (16) [which comes from the action along the supercritical trajectory (13)] is cubic.

If the condition $x(t) = X$ is specified at $t \neq T/2$, the solution becomes a bit more involved; we present it in Appendix D. Here the third-order dynamical phase transition occurs at a critical line $X_{c1}(t)$. Furthermore, the optimal trajectory becomes asymmetric around $T/2$ and an additional third-order transition occurs at a higher critical value $X_{c2}(t) > X_{c1}(t)$, similarly to the third-order transition, recently found in a different constrained Brownian motion [34]. In the subcritical regime $X \leq X_{c1}(t)$, Eqs. (14) and (15) give way to

$$-\ln \tilde{p}_A\left(z, \frac{t}{T}\right) \simeq \frac{A^2}{D_0 T^3} \frac{[z - \bar{z}(t)]^2}{2\sigma^2(t/T)}, \quad (17)$$

where $\bar{z}(t) = T x_A^*(t)/A$ [see Eq. (8)] and

$$\sigma^2(\xi) = \xi(1 - \xi)(3\xi^2 - 3\xi + 1). \quad (18)$$

These predictions also agree with simulations [see Fig. 2(b)]. As the excursions start and end at $x = 0$, the variance vanishes at $t = 0$ and $t = T$. More surprisingly, the variance (18) has a local minimum at $t = T/2$ and is maximal at $t = T(3 \pm \sqrt{3})/6$. The appearance of the local minimum of $\sigma^2(t/T)$ at $t = T/2$ is not exclusive to the large- A limit: We observed it in simulations for all values of \tilde{A} , but it is most prominent in the large- A tail.

As shown in Appendix D, in the subcritical regime $X \leq X_{c1}(t)$, the optimal trajectory is unaffected by the constraint at the origin for any t . This explains the coincidence of the Gaussian fluctuations in this regime [Eqs. (17) and (18)] with those of a Brownian bridge conditioned on A [42,43].

The two large-deviation formalisms, the DV method and the OFM, can be applied to other stochastic processes and dynamical observables. One example is the distribution $P(B, T)$ of the area under the square of a Brownian excursion $B = \int_0^T x^2(t) dt$. This distribution exhibits the scaling behavior $P(B, T) = D_0^{-1} T^{-2} h(B/D_0 T^2)$. We show in Appendix E how one can use the DV method and the OFM to obtain the tails of the scaling function $h(\dots)$, which were previously derived by probabilistic methods [22].

In conclusion, we presented the direct experimental measurements of the Airy distribution and of some of its large-deviation extensions. By exploiting the connection with two different large-deviation formalisms, we uncovered a relation of the AD with the Ferrari-Spohn distribution and found two dynamical phase transitions.

A promising future direction is to study the statistics of time-integrated quantities in multiparticle systems. For a large number of particles such systems can be efficiently probed with still another large-deviation technique: the rapidly developing macroscopic fluctuation theory [55].

B.M. was supported by the Israel Science Foundation (Grant No. 807/16). N.R.S. was supported by the Clore Israel Foundation.

APPENDIX A: EXPERIMENT, SIMULATIONS, AND THE VERVAAT TRANSFORM

Experiment and numerical simulations produce free Brownian trajectories rather than Brownian excursions. We obtained the latter from the former by applying two successive transformations (see, e.g., Ref. [40]). First, we employ a well-known mapping which transforms a free Brownian motion $x_{\text{Bm}}(t)$ into a Brownian bridge $x_{\text{Br}}(t)$ of duration T [56]:

$$x_{\text{Br}}(t) = x_{\text{Bm}}(t) - \frac{t}{T} x_{\text{Bm}}(T). \quad (A1)$$

Next we employ the Vervaat transform [57] which transforms a Brownian bridge into a Brownian excursion $x_{\text{ex}}(t)$. The Vervaat transform can be realized in three steps. First, place the origin at the absolute minimum attained by the bridge such that it is positive at all times. Next, shift the time by τ , the time at which the minimum was attained: $t \rightarrow t + \tau$. Finally, glue the first part of the trajectory from $t = 0$ to $t = \tau$ with the remainder of the trajectory from $t = \tau$ to $t = T$:

$$x_{\text{ex}}(t) = x_{\text{Br}}(t + \tau \bmod T) - x_{\text{Br}}(\tau). \quad (A2)$$

This procedure yields, in experiment and simulations, an ensemble of excursions with a prescribed duration T .

The mean position of excursions with a large and small area A was measured in the experiment and was found to agree well with the theoretical prediction as shown in Fig. 2(a). The full position distribution of excursions, conditioned on a given area, requires a considerably larger number of trajectories. It was easier to meet this requirement in simulations. In our simulations with the relatively large area under excursion, we used 5324 trajectories whose areas fit into the window $\tilde{A} = 1.2 \pm 0.0075$. These were extracted from a total of 2×10^7 Brownian excursions unconditioned by a specified area. Each trajectory was sampled along 1000 equally spaced points during its dynamics. For the small-area simulations, in the window $\tilde{A} = 0.3 \pm 0.0075$, we used 1885 trajectories. These were extracted from a total of 2×10^6 unconditioned Brownian excursions. Each trajectory here was sampled along 5000 equally spaced points. We verified the simulation method by measuring the area distribution of the excursions and comparing the results with the theoretical predictions (2) and (3). Very good agreement was observed. Very good agreement between the theory and the simulations is also evident for the mean position conditioned on the large and small area A , as shown in Fig. 5. On account of the very large number of simulated trajectories, the agreement here is better than that observed in Fig. 2(a).

APPENDIX B: THE DV FORMALISM AND THE SMALL- A TAIL

The DV formalism [25] reduces the problem of finding the rate function $I(a)$, defined in Eq. (6), in the large- T (or small- A) limit, to an effective eigenvalue problem. According to Gärtner and Ellis [26], the rate function $I(a)$ is given by a

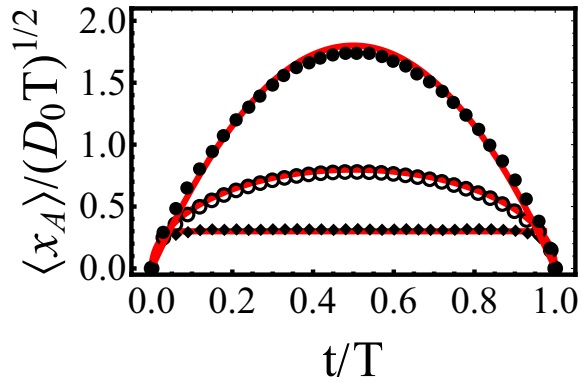


FIG. 5. Rescaled empirical position averages over simulated excursions, conditioned on a moderately large area $\tilde{A} = 1.2 \pm 0.0075$ (closed circles) and small area $\tilde{A} = 0.3 \pm 0.0075$ (closed diamonds). The top and bottom lines are theoretical predictions: Eq. (8) with $\tilde{A} = 1.2$ for the large area and the constant $\langle x_A \rangle / (D_0 T)^{1/2} \simeq \tilde{A} = 0.3$ for the small area. Also shown is the rescaled empirical average position of all (that is, unconstrained) excursions (open circles) and the theoretical prediction [29] $\langle x(t) \rangle / (D_0 T)^{1/2} = \sqrt{8/\pi} [(t/T)(1 - t/T)]^{1/2}$ (middle line).

Legendre-Fenchel transform

$$I(a) = \max_k [ka - \tilde{I}(k)] \quad (\text{B1})$$

of the scaled cumulant generating function (SCGF)

$$\tilde{I}(k) = \lim_{T \rightarrow \infty} \frac{1}{T} \ln \langle e^{Tka} \rangle, \quad (\text{B2})$$

where $\langle \cdot \cdot \cdot \rangle$ denotes averaging over values of a with respect to the Airy distribution (2). According to the DV method,

$$\tilde{I}(k) = \xi_{\max}(\hat{L}^{(k)}), \quad (\text{B3})$$

where ξ_{\max} is the maximal eigenvalue of the operator $\hat{L}^{(k)} \equiv \hat{L} + kx$, which is a tilted version of the Fokker-Planck generator \hat{L} , defined by the Fokker-Planck equation

$$\frac{\partial P(x, t)}{\partial t} = \hat{L}P(x, t), \quad (\text{B4})$$

corresponding to the Langevin equation for the stochastic process in question. For Brownian excursions the Fokker-Planck generator is just $\hat{L} = (D_0/2) \partial_x^2$ for $x > 0$ and $\hat{L} = -\infty$ for $x \leq 0$. It is convenient to convert the Fokker-Planck problem into an effective quantum mechanical one by considering the negative Fokker-Planck generator as an effective Hamiltonian, $\hat{H} \equiv -\hat{L}$, and look for the ground-state energy E_{\min} of the latter [27]. As a result,

$$\tilde{I}(k) = -E_{\min}(\hat{H}^{(k)}). \quad (\text{B5})$$

The effective Schrödinger equation for the Brownian excursion reads

$$-\frac{D_0}{2} \frac{d^2 \psi^{(k)}}{dx^2} - kx \psi^{(k)} = E^{(k)} \psi^{(k)}, \quad (\text{B6})$$

with the boundary conditions $\psi^{(k)}(0) = \psi^{(k)}(\infty) = 0$. The (discrete) spectrum, corresponding to Eq. (B6) with $k < 0$, is $E_n^{(k)} = (D_0/2)^{1/3} k^{2/3} \alpha_n$, where $n = 1, 2, \dots$ and α_n are the

absolute values of the zeros of the Airy function [19]. The corresponding eigenfunctions are

$$\psi_n^{(k)}(x) \propto \text{Ai}[-(2k/D_0)^{1/3} x - \alpha_n].$$

The SCGF is given by

$$\tilde{I}(k) = -(D_0/2)^{1/3} k^{2/3} \alpha_1. \quad (\text{B7})$$

Plugging this result into Eq. (B1) (and again assuming $k < 0$), we see that the maximum is achieved for

$$k(a) = -4D_0(\alpha_1/3a)^3, \quad (\text{B8})$$

and Eq. (B1) yields the small- A asymptotic (4) of the main text.

The solution of the tilted-generator problem also provides the conditional position distribution, associated with a prescribed rescaled area a . This distribution is given by the product of the left and right eigenfunctions of the tilted operator $\hat{L}^{(k)}$, corresponding to the maximal eigenvalue [45]. In our case the left and right eigenfunctions coincide due to the Hermiticity of the tilted operator and are both given by $\psi_1^k(x)$. Their properly normalized product gives the conditional position distribution that appears in Eq. (10), after the substitution of $k(a)$ from Eq. (B8).

APPENDIX C: MAPPING TO THE FERRARI-SPOHN MODEL

Ferrari and Spohn [48] studied the statistics of the position, at an intermediate time $t = t'$, of a Brownian bridge $x(t)$, when the process is constrained on staying away from an absorbing wall, that is $x(t) > x_w(t)$, where $x_w(t)$ is a semicircle, $x_w(t) = Ct^{1/2}(T - t)^{1/2}$. They also extended their results to other concave (that is, convex upward) functions. Ferrari and Spohn proved that at $T \rightarrow \infty$, typical fluctuations of $\Delta X = x(t') - x_w(t')$ away from the moving wall obey a universal distribution which depends only on the second derivative $\ddot{x}_w(t')$. This universal distribution can be represented as

$$P(\Delta X) = \frac{\ell \text{Ai}'(\ell \Delta X - \alpha_1)}{\text{Ai}'(-\alpha_1)^2}, \quad (\text{C1})$$

where $\text{Ai}(\dots)$ is the Airy function, $\alpha_1 = 2.338107\dots$ is the magnitude of its first zero, Ai' is the derivative of the Airy function with respect to its argument, and $\ell = [-2\ddot{x}_w(t')/D_0^2]^{1/3}$. Equation (C1) is valid in the limit $CT \gg \sqrt{D_0 T}$, which is when the wall “pushes” the Brownian bridge into the large-deviation regime.

Remarkably, Eq. (10), which describes the single-point distribution of a Brownian excursion conditioned on its covering a very small area $A \ll D_0^{1/2} T^{3/2}$, coincides with the distribution (C1) with $\ell = 2\alpha_1/3a$. This suggests that the model studied in the main text is related to the FS model. Indeed, we now establish a formal mapping between the two models and explain this coincidence.

The path integral that corresponds to the FS model is

$$\int Dx(t) e^{-s[x(t)]/D_0}, \quad (\text{C2})$$

constrained by $x(t=0) = x(t=T) = 0$ and $x(t) > x_w(t)$, where $s[x(t)]$ is the Wiener action, given by Eq. (7). Let us

define $y(t) = x(t) - x_w(t)$. Rewriting Eq. (C2) in terms of $y(t)$ (the Jacobian of this transformation is equal to 1), we obtain

$$\int Dy(t) e^{-\tilde{s}[y(t)]/D_0}, \quad (\text{C3})$$

where $y(t)$ are Brownian excursions, $y(t=0) = y(t=T) = 0$ and $y(t) > 0$, and the action is

$$\begin{aligned} \tilde{s}[y(t)] &= s[x_w(t) + y(t)] = s_0 + \frac{1}{2} \int_0^T (\dot{y}^2 + 2\dot{x}_w \dot{y}) dt \\ &= s_0 + \frac{1}{2} \int_0^T (\dot{y}^2 - 2\ddot{x}_w y) dt, \end{aligned} \quad (\text{C4})$$

where we used integration by parts and defined

$$s_0 = \frac{1}{2} \int_0^T \dot{x}_w^2 dt, \quad (\text{C5})$$

which is independent of $y(t)$. For the particular case of a parabolic wall $x_w(t) = Ct(1-t/T)$, we have $\ddot{x}_w(t) = -2C/T$, so Eq. (C4) becomes

$$\tilde{s}[y(t)] = s[y(t)] + \frac{2C}{T} \int_0^T y(t) dt + s_0. \quad (\text{C6})$$

The distribution of ΔX is given by

$$P_C(\Delta X) = \frac{\int Dy(t) e^{-\tilde{s}[y(t)]/D_0} \delta(y(t') - \Delta X)}{\int Dy(t) e^{-\tilde{s}[y(t)]/D_0}}, \quad (\text{C7})$$

where the C dependence enters through \tilde{s} . The constant s_0 is of no importance because its contributions cancel out. Equation (C7) is exact. In the large-deviation limit $CT \gg \sqrt{D_0 T}$, $P_C(\Delta X)$ is given by the FS distribution (C1) with

$$\ell = \left(\frac{4C}{D_0^2 T} \right)^{1/3}. \quad (\text{C8})$$

We now wish to find a connection between the FS model and the model studied in the present work. Let us begin by defining the canonical or biased ensemble [49]. This is an ensemble of excursions which is unconstrained by a specified A , but where the probability of each excursion is reweighted by the exponential factor $e^{-\mu A[x(t)]}$, where $A[x(t)]$ is the area of the excursion. The distribution of X in the canonical ensemble is given by

$$p(X; \mu) = \frac{\int Dx(t) e^{-s_\mu[x(t)]/D_0} \delta(x(t') - X)}{\int Dx(t) e^{-s_\mu[x(t)]/D_0}}, \quad (\text{C9})$$

where we defined the biased action

$$s_\mu[x(t)] = s[x(t)] + \mu D_0 \int_0^T x(t) dt. \quad (\text{C10})$$

Comparing Eqs. (C6) and (C7) with (C9) and (C10), we arrive at

$$P_C(\Delta X) = p\left(\Delta X; \mu = \frac{2C}{D_0 T}\right). \quad (\text{C11})$$

On the other hand, the canonical ensemble and the conditioned on A (or microcanonical) ensemble are equivalent and share the same relation as the one between canonical and microcanonical ensembles in equilibrium statistical mechanics [49]. In order to write this relation explicitly, we first

consider the joint probability density $\mathcal{P}(X, A)$ of $X = x(t')$ and A . It is related to the conditional probability via

$$\mathcal{P}(X, A) = P(A) p(X|A), \quad (\text{C12})$$

where $P(A)$ is given by the Airy distribution [see Eq. (3)]. Next we note that, up to a normalization constant, the joint probability of X and A in the canonical ensemble is simply $\mathcal{P}_\mu(X, A) \propto e^{-\mu A} \mathcal{P}(X, A)$. As a result, the relation between the two ensembles can be written as

$$p(X; \mu) = \frac{F(X, \mu)}{\mathcal{N}(\mu)}, \quad (\text{C13})$$

where

$$F(X, \mu) = \int_0^\infty e^{-\mu A} \mathcal{P}(X, A) dA \quad (\text{C14})$$

is the Laplace transform of $\mathcal{P}(X, A)$ with respect to A and

$$\mathcal{N}(\mu) = \int_0^\infty e^{-\mu A} P(A) dA \quad (\text{C15})$$

enforces the normalization condition $\int_0^\infty p(X; \mu) dX = 1$. Note that $\mathcal{N}(\mu)$ is the Laplace transform of $P(A)$ and it is known exactly [7,8]. Equations (C11)–(C15) provide an exact connection between the conditional probability distribution $p(X|A)$ and the distribution $P_C(\Delta X)$ in the Ferrari-Spohn model with a parabolic wall.

In the limit of $T \rightarrow \infty$ at fixed values of A/T and X (note that this limit implies a small area $A \ll D_0^{1/2} T^{3/2}$) the inverse Laplace transforms, which give $\mathcal{P}(X, A)$ and $P(A)$ from $F(X, \mu)$ and $\mathcal{N}(\mu)$, respectively, can be evaluated using the saddle-point approximation. This approximation is the basis of the DV formalism which we described in Appendix B. As a result, the conditional distribution can be written as

$$p(X|A) = \frac{\mathcal{P}(X, A)}{P(A)} \simeq \frac{e^{\mu^* A} F(X, \mu^*)}{e^{\mu^* A} \mathcal{N}(\mu^*)} = \frac{F(X, \mu^*)}{\mathcal{N}(\mu^*)}, \quad (\text{C16})$$

where $\mu^* = \mu^*(A)$ is found from the solution of the DV eigenvalue problem [see Eq. (B8)]:

$$\mu^* = -k = 4D_0 \left(\frac{\alpha_1 T}{3A} \right)^3. \quad (\text{C17})$$

Putting together Eqs. (C11), (C13), (C16), and (C17), we obtain

$$p(X|A) \simeq P_{C^*}(X), \quad (\text{C18})$$

where

$$C^* = \frac{\mu^* D_0 T}{2} = \frac{2\alpha_1^3 D_0^2 T^4}{27A^3}. \quad (\text{C19})$$

Now, since

$$\frac{C^* T}{\sqrt{D_0 T}} = \frac{2\alpha_1^3}{27} \left(\frac{D_0^{1/2} T^{3/2}}{A} \right)^3 \gg 1,$$

$P_{C^*}(X)$ in Eq. (C18) is given by the FS distribution (C1), with $\ell = 2\alpha_1 T/3A$, which is found by plugging Eq. (C19) into Eq. (C8). This indeed leads to a coincidence of Eq. (C18) with Eq. (10). We recall that the coincidence occurs in the limit of $T \rightarrow \infty$ at fixed values of A/T and X . Larger deviations in the two models (when T is fixed and we consider the large- ΔX

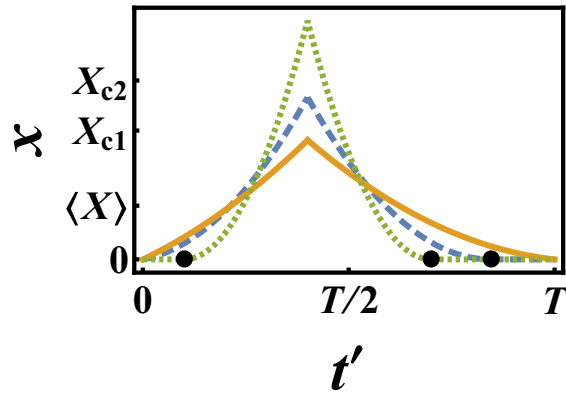


FIG. 6. Optimal paths conditioned on $x(t = 0.4T) = X$ and the area A , in the subcritical (solid), intermediate (dashed), and supercritical (dotted) regimes [see Eqs. (D2), (D4), and (D6)]. The parameters are $XT/A = 2.5, 3.4,$ and 5 (solid, dashed, and dotted lines, respectively). Circles show the times when $x(t)$ vanishes: $t' = \tau$ for the intermediate trajectory [see Eqs. (D4) and (D5)] and $|t - t'| = 3A/2X$ for the supercritical trajectory.

or large- X limit) behave differently [see Eqs. (14)–(16) and Ref. [34]].

APPENDIX D: THE OFM AND THE LARGE-A TAIL

The conditional probability distribution $p(X, t|A \gg \sqrt{D_0 T^3})$ is given by the ratio of the probability of the Brownian excursion realizing a specified area A and the constraint $x(t) = X$ and the probability of it realizing the area A alone. Within the OFM, these probabilities are given by the path probability measures of the optimal Brownian excursion $x(t')$ realizing the large A with and without the additional constraint $x(t) = X$. The latter is accommodated into the OFM minimization problem via an additional Lagrange multiplier λ_2 leading to the effective Lagrangian $L[x(t'), \dot{x}(t')] = \dot{x}^2/2 - \lambda x - \lambda_2 \delta(t' - t)$, where $\delta(\dots)$ is the delta function [34]. There are three regimes of interest, the subcritical, the intermediate, and the supercritical, separated by two third-order dynamical phase transitions, as we now describe.

In the subcritical regime $0 < X \leq X_{c1}$, where

$$X_{c1}(t) = \frac{6(\frac{T}{2} + |\frac{T}{2} - t|)^2 A}{(3|\frac{T}{2} - t| + \frac{T}{2})T^2}, \tag{D1}$$

the optimal trajectory is composed of two parabolic segments with a discontinuous derivative at $t' = t$. For $0 \leq t' \leq t$ the trajectory is given by

$$x(t') = \frac{t'[X(T^2 - 3tT) + 6at^2 - t'(6at - 3Xt)]}{t(T^2 - 3tT + 3t^2)}. \tag{D2}$$

For $t \leq t' \leq T$ one should replace here t and t' by $T - t$ and $T - t'$, respectively. This trajectory is shown by the solid line in Fig. 6.

In the particular case of $t = T/2$ the trajectory is symmetric around $T/2$ [see Eq. (12)]. The conditional probability is given by the difference in the actions [Eq. (7)] along the trajectory (D2) and the trajectory given by Eq. (8), which is

conditioned by the area A alone. Here we obtain a Gaussian distribution

$$-\ln p(X, t|A \gg \sqrt{D_0 T^3}) \simeq \frac{\Delta s}{D_0} = \frac{[X - x_A^*(t)]^2}{2D_0 T \sigma^2(t)}, \tag{D3}$$

where $\sigma^2(t)$ and $x_A^*(t)$ are given by Eqs. (18) and (8), respectively.

When X exceeds X_{c1} , $x(t')$ from Eq. (D2) would cross the origin. For $t < T/2$ ($t > T/2$) this happens first at the right (left) end of the trajectory $t' = T$. A solution crossing the origin is not allowed and the correct solution in this intermediate regime is given by the tangent construction of the calculus of one-sided variations [54]. This solution vanishes identically past a point τ which we now determine. For concreteness, let us assume that $0 < t < T/2$. (The case $T/2 < t < T$ is obtained from symmetry.) In this regime, $X_{c1} \leq X \leq X_{c2} \equiv 3A/2t$, the optimal trajectory is

$$x(t') = \frac{X}{(\tau - t)^2} \times \begin{cases} 0, & \tau \leq t' \leq T \\ (\tau - t')^2, & t \leq t' \leq \tau \\ t'^2 + \frac{(\tau - t)^2 - t'^2}{t}, & 0 \leq t' \leq t, \end{cases} \tag{D4}$$

where τ is given by

$$\frac{\tau}{t} = \frac{(2\tilde{a} - 1)^2}{2[\sqrt{(2\tilde{a} - 1)^3 + 1} + 1]^{2/3}} + \frac{1}{2}[\sqrt{(2\tilde{a} - 1)^3 + 1} + 1]^{2/3} + \tilde{a} + \frac{1}{2}, \tag{D5}$$

where $\tilde{a} \equiv A/Xt$. This trajectory is shown by the dashed line in Fig. 6.

In the supercritical regime $X \geq X_{c2}$, the trajectory (D4) also becomes invalid, as it crosses the origin. Now this happens immediately: at $t' = 0$. Again, the tangent construction is needed in order to find the valid optimal trajectory. This time the correct $x(t)$ vanishes at two points along the trajectory:

$$x(t') = \begin{cases} \frac{4X^3}{9A^2} (\frac{3A}{2X} - |t - t'|)^2, & |t - t'| \leq \frac{3A}{2X} \\ 0, & |t - t'| \geq \frac{3A}{2X}. \end{cases} \tag{D6}$$

This expression, which is a simple extension of Eq. (13) to $t \neq T/2$, is shown by the dotted line in Fig. 6.

At each of the two critical lines $X = X_{c1}(t)$ and $X = X_{c2}(t)$ a third-order dynamical phase transition occurs, corresponding to a jump in the third derivative of the large-deviation function with respect to X . At $X_{c1} \leq X \leq X_{c2}$ the large-deviation function is given by

$$-\ln p(X, t|A \gg \sqrt{D_0 T^3}) \simeq \frac{\Delta s}{D_0} = \frac{6A^2}{D_0} \left[\frac{3\tau^2 - 8t\tau + 6t^2}{t\tau^2(2\tau - 3t)^2} - \frac{1}{T^3} \right], \tag{D7}$$

where τ is given by (D5), while at $X \geq X_{c2}$ the large-deviation function is given by

$$-\ln p(X, t|A \gg \sqrt{D_0 T^3}) \simeq \frac{\Delta s}{D_0} = \frac{A^2}{D_0} \left(\frac{8X^3}{9A^3} - \frac{1}{T^3} \right). \tag{D8}$$

For the particular case $t = T/2$ the two dynamical phase transitions merge into a single third-order transition, as described in the main text.

APPENDIX E: AREA UNDER THE SQUARE OF BROWNIAN EXCURSION

Here we study the probability distribution $P(B, T)$ of the area under the square of a Brownian excursion

$$B = \int_0^T dt x^2(t). \quad (\text{E1})$$

Dimensional analysis yields the scaling form

$$P(B, T) = \frac{1}{D_0 T^2} h\left(\frac{B}{D_0 T^2}\right).$$

For convenience we will set $D_0 = 1$ and restore the D_0 dependence in the final results. The Laplace transform of $P(B, T)$, $\tilde{P}(\lambda, T) = \int_0^\infty P(B, T) e^{-\lambda B} dB$, was derived in Ref. [58] by probabilistic methods. For completeness, we present here a simpler and more physical derivation by using path-integral methods. Our main focus, however, is the small- and large- B tails of $P(B, T)$ and their intrinsic connections to the DV method and the OFM, respectively.

The probability distribution $P(B, T)$ is given by a sum over all the Brownian excursions on the interval $0 < t < T$, conditioned by Eq. (E1). There is a subtlety here: A Brownian particle, starting at the origin, would cross it infinitely many times immediately afterward and would not stay positive as required. This difficulty is circumvented by introducing a cutoff: assuming that $x(0) = x(T) = \epsilon > 0$ and sending ϵ to zero at the end of the calculation (see, e.g., Ref. [13]). That is,

$$\tilde{P}(\lambda, T) = \lim_{\epsilon \rightarrow 0} \left\langle \exp\left(-\lambda \int_0^T d\tau x^2(\tau)\right) \right\rangle_\epsilon, \quad (\text{E2})$$

where $\langle \dots \rangle_\epsilon$ denotes the expectation value over realizations of Brownian motions which satisfy $x(0) = x(T) = \epsilon$ and stay positive for $0 < t < T$. The expectation value is given by

$$\begin{aligned} & \left\langle \exp\left(-\lambda \int_0^T d\tau x^2(\tau)\right) \right\rangle_\epsilon \\ &= \frac{1}{Z(\epsilon, T)} \int_{x(0)=\epsilon}^{x(T)=\epsilon} \mathcal{D}x(\tau) \\ & \times \exp\left\{-\int_0^T d\tau \left[\frac{1}{2} \left(\frac{\partial x}{\partial \tau}\right)^2 + \lambda x^2(\tau)\right]\right\} \\ & \times \prod_{\tau=0}^T \theta[x(\tau)] = \frac{G_\lambda(\epsilon, T|\epsilon, 0)}{Z(\epsilon, T)}, \end{aligned} \quad (\text{E3})$$

where the normalization constant $Z(\epsilon, T) = \tilde{P}(0, T)$ is the probability of a Brownian excursion unconstrained by B . The propagator $G_\lambda(\epsilon, T|\epsilon, 0)$ is given by the quantum mechanical expectation value $\langle \epsilon | e^{-\hat{H}^{(\lambda)} T} | \epsilon \rangle$, with the Hamiltonian $\hat{H}^{(\lambda)} = -(1/2) \partial_x^2 + \lambda V(x)$, where the potential is given by $V(x > 0) = x^2$ and $V(x \leq 0) = \infty$. The normalization constant $Z(\epsilon, T)$ can be obtained either by solving the diffusion equation with an absorbing boundary condition at the origin [59] or by applying the Feynman-Kac formula [12], which

reduces the problem to finding the propagator $G_0(\epsilon, T|\epsilon, 0) = \langle \epsilon | e^{-\hat{H}_1} | \epsilon \rangle$, where $\hat{H}_1 = -(1/2) \partial_x^2 + V(x)$, with $V(x > 0) = 0$ and $V(x \leq 0) = \infty$. Both methods yield

$$Z(\epsilon, T) = \frac{1}{\sqrt{2\pi T}} (1 - e^{-2\epsilon^2/T}). \quad (\text{E4})$$

Let us calculate the propagator $G_\lambda(\epsilon, T|\epsilon, 0)$. Here $\hat{H}^{(\lambda)}$ is the Hamiltonian of a harmonic oscillator, where $\hbar = m = 1$ and $\omega^2 = 2\lambda > 0$. Because of the absorbing boundary condition at $x = 0$, only the odd eigenfunctions (the Gauss-Hermite functions [60]) are present. The spectrum is given by $E_{2k+1} = \sqrt{2\lambda}(2k + 3/2)$. The propagator G_λ can be expanded in this basis

$$\begin{aligned} G_\lambda(\epsilon, t|\epsilon, 0) &= \langle x = \epsilon | e^{-\hat{H}^{(\lambda)} T} | x = \epsilon \rangle \\ &= \sum_{k=0}^{\infty} |\psi_{2k+1}(\epsilon)|^2 e^{-\sqrt{2\lambda}(2k+3/2)T}, \end{aligned} \quad (\text{E5})$$

where the Gauss-Hermite functions, normalized to unity over the region $x \in [0, \infty)$, are [60]

$$\psi_{2k+1}(\epsilon) = \frac{\sqrt{2}}{\sqrt{2^{2k+1}(2k+1)!}} \left(\frac{\omega}{\pi}\right)^{1/4} e^{-\omega\epsilon^2/2} H_{2k+1}(\sqrt{\omega}\epsilon), \quad (\text{E6})$$

where $H_{2k+1}(\dots)$ are the Hermite polynomials and $\omega^2 = 2\lambda$. Before we send ϵ to zero, we evaluate Eq. (E6) at small ϵ . The small-argument asymptotic of H_{2k+1} [61] can be written as

$$H_{2k+1}(\epsilon) \simeq \frac{(-1)^k (2k+2)!}{(k+1)!} \epsilon. \quad (\text{E7})$$

Plugging this asymptotic into the Gauss-Hermite functions (E6), we obtain

$$\psi_{2k+1}(\epsilon) \simeq \frac{(-1)^k \sqrt{(2k+1)!}}{2^{k-1} k!} \left(\frac{\omega}{\pi}\right)^{1/4} \sqrt{\omega}\epsilon. \quad (\text{E8})$$

Using this expression in (E5), we can perform the summation exactly:

$$\begin{aligned} G_\lambda(\epsilon, T|\epsilon, 0) &\simeq \epsilon^2 \sum_{k=0}^{\infty} \frac{(2k+1)! e^{-\sqrt{8\lambda}Tk}}{2^{2k-2} (k!)^2} e^{-\sqrt{9\lambda}/2 T} \left[\frac{(2\lambda)^3}{\pi^2}\right]^{1/4} \\ &= \epsilon^2 \frac{4e^{-\sqrt{9\lambda}/2 T}}{(1 - e^{-\sqrt{8\lambda}T})^{3/2}} \left[\frac{(2\lambda)^3}{\pi^2}\right]^{1/4}. \end{aligned} \quad (\text{E9})$$

Using Eq. (E4), we can now calculate the propagator $\tilde{P}(\lambda, T) = \lim_{\epsilon \rightarrow 0} [G_\lambda(\epsilon, T)/Z(\epsilon, T)]$. Restoring the D_0 dependence, we finally obtain

$$\tilde{P}(\lambda, T) = \left[\frac{\sqrt{2D_0\lambda T}}{\sinh(\sqrt{2D_0\lambda T})} \right]^{3/2}, \quad (\text{E10})$$

in agreement with Ref. [58]. To our knowledge, the inverse Laplace transform of Eq. (E10) is unknown in analytical form. We performed the inversion numerically (see Fig. 7) using a multiprecision inverse Laplace transform algorithm [62], realized in *Mathematica*.

We will now derive the small- and large- B tails of the distribution $P(B, T)$. Instead of extracting them from the exact Laplace transform (E10), we will directly employ the DV

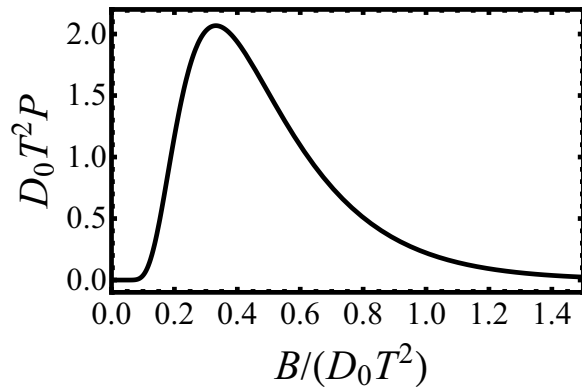


FIG. 7. Rescaled probability distribution $P(B, T)$ of the area B under the square of a Brownian excursion.

formalism for small B and the OFM for large B . As we will see, these calculations turn out to be quite simple.

1. Small- B tail of $P(B, T)$

By virtue of Eq. (B5) for $\hat{H}^{(k)} \equiv \hat{H}^{(-\lambda)}$, we obtain

$$\tilde{I}(k) = -\sqrt{\frac{-9k}{2}}, \quad (\text{E11})$$

where $k < 0$. The Legendre-Fenchel transform (B1) yields the DV rate function

$$I(b) = \frac{9}{8b}, \quad (\text{E12})$$

where $b \equiv B/T$. This leads to

$$-\ln P(B \ll D_0 T^2) \simeq \frac{9D_0 T^2}{8B}, \quad (\text{E13})$$

in agreement with Ref. [22].

2. Large- B tail of $P(B, T)$

The constrained Lagrangian of the OFM is now $L[x(t), \dot{x}(t)] = \dot{x}^2/2 - \lambda x^2$. The optimal trajectory is

$$x(t) = \sqrt{\frac{2B}{T}} \sin\left(\frac{\pi t}{T}\right), \quad (\text{E14})$$

where we set $\lambda = \pi^2/2T^2$ to obey the constraint $B = \int_0^T x^2(t) dt$. Calculating the action from Eq. (7), we finally obtain

$$-\ln P(B \gg D_0 T^2) \simeq \frac{\pi^2 B}{2D_0 T^2}, \quad (\text{E15})$$

in agreement with Ref. [22].

-
- [1] A. Einstein, *Ann. Phys. (Leipzig)* **322**, 549 (1905).
 [2] M. von Smoluchowski, *Ann. Phys. (Leipzig)* **326**, 756 (1906).
 [3] P. Langevin, *C. R. Acad. Sci. (Paris)* **146**, 530 (1908).
 [4] J. Perrin, *C. R. Acad. Sci. (Paris)* **146**, 967 (1908).
 [5] S. N. Majumdar, *Curr. Sci.* **89**, 2076 (2005).
 [6] R. M. Mazo, *Brownian Motion: Fluctuations, Dynamics, and Applications* (Oxford Science, Oxford, 2008).
 [7] D. A. Darling, *Ann. Probab.* **11**, 803 (1983).
 [8] G. Louchard, *J. Appl. Probab.* **21**, 479 (1984).
 [9] L. Takács, *J. Appl. Math. Stoch. Anal.* **4**, 363025 (1991).
 [10] L. Takács, *Adv. Appl. Prob.* **23**, 557 (1991); *J. Appl. Prob.* **32**, 375 (1995).
 [11] P. Flajolet, P. Pobleto, and A. Viola, *Algorithmica* **22**, 490 (1998).
 [12] S. N. Majumdar and A. Comtet, *Phys. Rev. Lett.* **92**, 225501 (2004).
 [13] S. N. Majumdar and A. Comtet, *J. Stat. Phys.* **119**, 777 (2005).
 [14] G. Schehr and S. N. Majumdar, *Phys. Rev. E* **73**, 056103 (2006).
 [15] M. A. Stapleton and K. Christensen, *J. Phys. A: Math. Gen.* **39**, 9107 (2006).
 [16] S. Medalion, E. Aghion, H. Meirovitch, E. Barkai, and D. A. Kessler, *Sci. Rep.* **6**, 27661 (2016).
 [17] E. Barkai, E. Aghion, and D. A. Kessler, *Phys. Rev. X* **4**, 021036 (2014).
 [18] Wolfram Research, Inc., <http://functions.wolfram.com/HypergeometricFunctions/>.
 [19] O. Vallée and M. Soares, *Airy Functions and Applications to Physics* (Imperial College, London, 2004).
 [20] S. Janson, *Probab. Surveys* **4**, 80 (2007).
 [21] M. J. Kearney, S. N. Majumdar, and R. J. Martin, *J. Phys. A: Math. Theor.* **40**, F863 (2007).
 [22] M. Csörgö, Z. Shi, and M. Yor, *Bernoulli* **5**, 1035 (1999).
 [23] P. Flajolet and G. Louchard, *Algorithmica* **31**, 361 (2001).
 [24] J. C. Crocker and D. G. Grier, *J. Colloid Interface Sci.* **179**, 298 (1996).
 [25] M. D. Donsker and S. R. S. Varadhan, *Commun. Pure Appl. Math.* **28**, 1 (1975); **28**, 279 (1975); **29**, 389 (1976); **36**, 183 (1983).
 [26] J. Gärtner, *Theor. Prob. Appl.* **22**, 24 (1977); R. S. Ellis, *Ann. Prob.* **12**, 1 (1984).
 [27] H. Touchette, *Phys. Rep.* **478**, 1 (2009).
 [28] H. Touchette, *Physica A* **504**, 5 (2018).
 [29] F. Colaiori, A. Baldassarri, and C. Castellano, *Phys. Rev. E* **69**, 041105 (2004).
 [30] A. Grosberg and H. Frisch, *J. Phys. A: Math. Gen.* **36**, 8955 (2003).
 [31] N. Ikeda and H. Matsumoto, in *Memoriam Marc Yor: Séminaire de Probabilités XLVII*, edited by C. Donati-Martin, A. Lejay, and A. Rouault, Lecture Notes in Mathematics Vol. 2137 (Springer, Cham, 2015), p. 497.
 [32] K. Basnayake, A. Hubl, Z. Schuss, and D. Holcman, *Phys. Lett. A* **382**, 3449 (2018).
 [33] B. Meerson, *J. Stat. Mech.* (2019) 013210.
 [34] N. R. Smith and B. Meerson, *J. Stat. Mech.* (2019) 023205.
 [35] B. Meerson and N. R. Smith, *J. Phys. A: Math. Theor.* **52**, 415001 (2019).
 [36] B. Meerson, *Int. J. Mod. Phys. B* **33**, 1950172 (2019).
 [37] J. A. Fill and S. Janson, *Ann. Comb.* **12**, 403 (2009).
 [38] S. Janson and G. Louchard, *Electron. J. Probab.* **12**, 1600 (2007).

- [39] J. L. Doob, *Classical Potential Theory and its Probabilistic Counterpart* (Springer, New York, 1984).
- [40] S. N Majumdar and H. Orland, *J. Stat. Mech.* (2015) P06039.
- [41] S. N. Majumdar and C. Dasgupta, *Phys. Rev. E* **73**, 011602 (2006).
- [42] A. Mazzolo, *J. Stat. Mech.* (2017) 023203.
- [43] A. Mazzolo, *J. Math. Phys.* **58**, 093302 (2017).
- [44] T. Sottinen and A. Yazigi, *Stoch. Process. Appl.* **124**, 3084 (2014).
- [45] R. Chetrite and H. Touchette, *Ann. Henri Poincaré* **16**, 2005 (2015).
- [46] P. Groeneboom, *Probab. Theory Relat. Fields* **81**, 79 (1989).
- [47] L. Frachebourg and P. Martin, *J. Fluid Mech.* **417**, 323 (2000).
- [48] P. L. Ferrari and H. Spohn, *Ann. Probab.* **33**, 1302 (2005).
- [49] R. Chetrite and H. Touchette, *Phys. Rev. Lett.* **111**, 120601 (2013).
- [50] D. Ioffe, S. Shlosman, and Y. Velenik, *Commun. Math. Phys.* **336**, 905 (2015).
- [51] D. Ioffe, Y. Velenik, and V. Wachtel, *Probab. Theory Relat. Fields* **170**, 11 (2018).
- [52] D. Ioffe and Y. Velenik, *Markov Process. Relat. Fields* **24**, 487 (2018).
- [53] S. Nechaev, K. Polovnikov, S. Shlosman, A. Valov, and A. Vladimirov, *Phys. Rev. E* **99**, 012110 (2019).
- [54] L. Elsgolts, *Differential Equations and the Calculus of Variations* (Mir, Moscow, 1977), p. 360.
- [55] L. Bertini, A. De Sole, D. Gabrielli, G. Jona-Lasinio, and C. Landim, *Rev. Mod. Phys.* **87**, 593 (2015).
- [56] W. Feller, *An Introduction to Probability Theory and its Applications* (Wiley, New York, 1968).
- [57] W. Vervaat, *Ann. Probab.* **7**, 143 (1979).
- [58] M. Nguyen, *Combin. Probab. Comput.* **13**, 697 (2004).
- [59] S. Redner, *A Guide to First-Passage Processes* (Cambridge University Press, Cambridge, 2001).
- [60] L. D. Landau and E. M. Lifshitz, *Quantum Mechanics, Non-Relativistic Theory* (Pergamon, London, 1958).
- [61] Wolfram Research, Inc., <http://mathworld.wolfram.com/HermitePolynomial.html>.
- [62] J. Abate and P. P. Valkó, *Int. J. Numer. Methods Eng.* **60**, 979 (2004).